A Survey of Supersonic Retropropulsion Technology for Mars Entry, Descent, and Landing[1,2]

Ashley M. Korzun
Georgia Institute of Technology
Atlanta, GA 30332-0150
(404) 894-7783
akorzun@gatech.edu

Juan R. Cruz
NASA Langley Research Center
Hampton, VA 23681-2199
(757) 864-3173
Juan.R.Cruz@nasa.gov

Robert D. Braun
Georgia Institute of Technology
Atlanta, GA 30332-0150
(404) 385-6171
robert.braun@ae.gatech.edu

Abstract—This paper presents a literature survey on supersonic retropropulsion technology as it applies to Mars entry, descent, and landing (EDL). The relevance of this technology to the feasibility of Mars EDL is shown to increase with ballistic coefficient to the point that it is likely required for human Mars exploration. The use of retropropulsion to decelerate an entry vehicle from hypersonic or supersonic conditions to a subsonic velocity is the primary focus of this review. Discussed are systems-level studies, general flowfield characteristics, static aerodynamics, vehicle and flowfield stability considerations, and aerothermodynamics. The experimental and computational approaches used to develop retropropulsion technology are also reviewed. Finally, the applicability and limitations of the existing literature and current state-of-the-art computational tools to future missions are discussed in the context of human and robotic Mars exploration.

TABLE OF CONTENTS

1 INTRODUCTION

In most current EDL systems, decelerating the vehicle from hypersonic to subsonic speeds is achieved using the aerodynamic drag of the entry vehicle and other aerodynamic decelerators such as parachutes [1]. At Mars, high entry masses and insufficient atmospheric density often result in unacceptable parachute deployment and operating conditions. An alternative deceleration approach is to initiate retropropulsion while the vehicle is still traveling supersonically. Supersonic retropropulsion may be an enabling technology for systems with high ballistic coefficients operating in thin atmospheres such as at Mars.

Investigation into the interaction of supersonic retropropulsion with blunt body aerodynamics began in the early 1950s. Experimental work with small-scale wind tunnel models by Love [2],[3],[4], Huff and Abdalla [5], and Moeckel [6],[7] focused on shock-boundary layer phenomena and the effects of nozzle flow on boundary layer transition. These investigations were among the earliest observations of the aerodynamic drag reductions and associated flowfield stability transitions for configurations with a nozzle located along the body centerline. Moeckel [6],[7] was among the first to observe an aerodynamic drag reduction in supersonic retropropulsion configurations with a centerline nozzle application. Moeckel [6],[7] also observed flow separation on the forebody with the same configuration. Both effects were later observed in other experiments with a supersonic retropropulsion nozzle along the centerline of a blunt entry body [15],[18]-[21],[23]-[28],[34]-[35],[37],[39]-[41].

These early works are consistent in observing that increasing thrust coefficient (defined in Eq. 1) moves the boundary layer transition closer to the nose of the body [2]. Additional work [4],[5],[8],[9] on supersonic jet flow and jet-body interactions laid the groundwork for future wind tunnel testing of supersonic nozzle exhaust effects on body surface pressure distributions and flowfield stability. While many of these body shapes were not the blunted-cone entry vehicle shapes flown in the 1960s and 1970s, these works established the fundamental physics of shock-boundary layer interactions and motivated later investigations to apply such interaction effects to blunt body entry vehicles for planetary exploration.

This early retropropulsion work was extended to blunt body entry geometries in the 1960s and early 1970s, primarily through wind tunnel experiments on small-scale models. Among the concepts investigated were single and multiple nozzle configurations, with the retropropulsion nozzles placed at either the center or the periphery of the vehicle forebody. Experimental results for low thrust coefficients consistently show significant increases in the total axial force coefficient (summation of aerodynamic drag and thrust) for peripheral nozzle locations [15],[25]-[26]. In contrast, aerodynamic drag reduction was observed for centerline nozzle locations [15],[18]-[21],[23]-[25],[27]-[28],[34]-[35],[37],[39]-[41] . For high thrust coefficients, all nozzle configurations contributed substantially to the effective total axial force on the vehicle, though by thrust

---

contributions only (no aerodynamic drag contribution) [15],[18],[20]-[21],[23]-[24],[26]-[27]. Additionally, the stability of the flowfield and resulting aerodynamic effects were found to be strongly dependent on the ratio of total pressure between the retropropulsion and the freestream [15],[18]-[21],[23]-[28],[34]-[35],[37],[39]-[41].

Although the majority of the literature is focused on deceleration applications, the aerothermal effects of supersonic retropropulsion, the development of test scaling parameters, and the capabilities of computational analysis have also been explored [15],[19],[21],[34]-[45]. Both experimental and computational work show the aerothermal effects of retropropulsion to be important, with the potential for heat transfer to the body to be doubled when combustion products are injected into the shock layer.

Experimental work has produced relationships for scaling and developed the primary similarity parameters for model and nozzle design. Computational investigation has recently been renewed and early code validation efforts with show good agreement with experimental data for axisymmetric configurations. While computational solutions are in agreement with experimental data for stable flowfield conditions, these computational models may be unable to accurately capture the complete physical behavior for unstable flowfield conditions.

This paper provides a survey of the literature on the effects of retropropulsion on blunt body entry vehicles in an opposing supersonic or hypersonic freestream. The focus is on aerodynamic performance effects for application to EDL design and computational simulation development. This paper does not discuss non-propulsive supersonic decelerators, reaction control system interactions, slender-body geometries, or exhaust plumes in directions other than against the freestream. Section 2 discusses past Mars EDL systems studies and the retropropulsion sizing models used in those analyses. Sections 3 – 6 compare central and peripheral nozzle locations, as well as the effects of variations in environment and design parameters such as nozzle geometry and chemical composition of the freestream and retrorocket exhaust. Section 7 discusses the computational simulation of supersonic retropropulsion flowfields and the extensibility and limitations of this work.

2 RETROPROPULSION SYSTEMS STUDIES

To date, the United States has successfully landed five robotic missions on Mars: Viking 1, Viking 2, Mars Pathfinder, and the two Mars Exploration Rovers. Including missions launched by the end of the decade, the largest payload mass landed on Mars will be Mars Science Laboratory (MSL), whose rover is approaching 900 kg. The EDL systems for these missions rely heavily on extensions of Viking-heritage technology, namely supersonic Disk-Gap-Band (DGB) parachutes, 70º sphere-cone blunt body aeroshells, and subsonic propulsive terminal descent [1].

The focused technology development program preceding the Viking missions in the 1960s and 1970s developed supersonic retropropulsion to nearly the level of maturity the concept has today. The eventual selection of a supersonic DGB parachute system and subsonic propulsive terminal descent phase for the Viking landers ended much of the research efforts to develop supersonic retropropulsion. Only recently has interest in supersonic retropropulsion resurfaced. The applicability of Viking EDL technologies to the high mass planetary entries needed for human Mars exploration has been shown to be constrained by deployment conditions and performance at higher Mach numbers of supersonic DGB parachutes [1]. This resurgence of interest in human Mars exploration has resulted in systems-level studies to assess the required performance of these high-mass entry systems, and the conclusions of these studies, in general, recommend the development of alternative supersonic decelerators, a challenge potentially addressed by supersonic retropropulsion.

Human Mars architecture studies [10],[11],[12],[13] predict payload masses on the order of 20 to 100 t. The EDL requirements of these high-mass, high ballistic coefficient systems extend well beyond the capabilities of many Viking-heritage EDL technologies. Supersonic deceleration is possibly the most critical deficiency in extending these heritage technologies. The high ballistic coefficients in these architecture studies (~300 kg/m^2 and higher), thin Mars atmosphere, and inability to extend supersonic DGB parachutes to the required dimensions and deployment conditions severely reduce the timeline available for deceleration and the transition from a hypersonic entry vehicle to a terminal landing configuration.

The point design in NASA's 1998 Mars Design Reference Mission [10],[11] attempts to address the supersonic deceleration gap by using clusters of 50 m diameter supersonic parachutes, followed by a subsonic propulsive terminal descent. Alternatively, Christian, et al. [12] replaced the traditional parachute system with a purely propulsive descent, initiated at supersonic velocities. Because these studies are for human class missions, with payload masses ranging from 20 to 100 t, significantly larger propulsion systems are required than have been flown previously. In these studies, the descent propulsion systems for supersonic deceleration have been assumed to be LOX/methane RD-180 derivatives, with an engine thrust to weight (*T/W*) of 80 and maximum thrust of 1 MN [12],[14]. A thrust magnitude of 1 MN for an RD-180 derivative engine corresponds to a thrust coefficient of approximately 0.9. The thrust coefficient is defined as the ratio of the thrust, *T*, to the nozzle operating pressure, p_0, and throat area, A^*:

$$C_T = \frac{T}{p_0 A^*} \qquad (1)$$

For a retropropulsion configuration where the nozzles are

located on the forebody periphery, the maximum increase in total axial force coefficient (aerodynamic drag and thrust contributions) occurs near conditions corresponding to a thrust coefficient of 1.0 [15]. Hence, proper modeling of the supersonic retropropulsion system can have a dramatic impact on EDL architectural performance. These aerodynamic effects are discussed in Section 4.

Prior robotic Mars missions have had vehicle T/W values on the order of 3 [1]. For three payload cases (20, 40, and 70 t) [11] and a fixed maximum thrust magnitude of 1.0 MN, the required vehicle T/W and thrust coefficient can be significantly different from robotic missions as payload mass increases (i.e., $T/W \approx 2.3$ or 1.5 vs. 3.0). The trajectories from Christian, et al. [12] have limited the maximum deceleration to 5 g's during descent, translating into varying required thrust levels to slow the vehicle to subsonic velocities. Table 1a gives the required vehicle T/W and thrust coefficient for a fixed maximum thrust (T_{max}) for payload masses of 20, 40, and 70 t. Table 1b gives the required maximum thrust and thrust coefficient for a fixed vehicle T/W of 3.0 for these three payload masses.

Table 1. T/W Comparison for Human Mars Missions

(a.)

Payload Mass (t)	Entry Mass (t)	Fixed Max Thrust		
		T_{max}	T/W	C_T
20	79	1.0 MN	3.40	0.87
40	115	1.0 MN	2.33	0.87
70	176	1.0 MN	1.52	0.87

(b.)

Payload Mass (t)	Entry Mass (t)	Fixed T/W		
		T/W	T_{max}	C_T
20	79	3.0	0.88 MN	0.77
40	115	3.0	1.29 MN	1.12
70	176	3.0	1.97 MN	1.72

Of these architectural studies, only the investigations by Christian, and Wells, et al. [12],[13] initiate retropropulsion at supersonic speeds. In these references, the aerodynamic interaction of supersonic retropropulsion was not modeled (i.e., the deceleration was assumed to be independent of nozzle location). In addition, the aerodynamic drag was set to zero, and only the axial force due to thrust was modeled. Past experimental evidence suggests that, for configurations with the nozzles located at the forebody periphery, inclusion of aerodynamic interaction effects into supersonic retropropulsion performance models will reduce the propellant mass required.

The relationship between descent propellant mass fraction required and payload mass is shown in Figure 1. The figure illustrates the increasing impact of aerodynamic effects on required descent propellant mass fraction as ballistic coefficient increases. If the supersonic ΔV can be reduced

by 30%, due to augmentation of the total axial force coefficient, the descent propellant mass fraction can be reduced by 15% or more. An example case is a 15 m diameter, 60 t vehicle with a ballistic coefficient of approximately 250 k/m^2 and 4 RD-180 derivative engines around the periphery of the forebody [12]. A 30% reduction in the supersonic ΔV reduces the descent propellant mass fraction from 0.137 to 0.116, a difference of 16.5%.
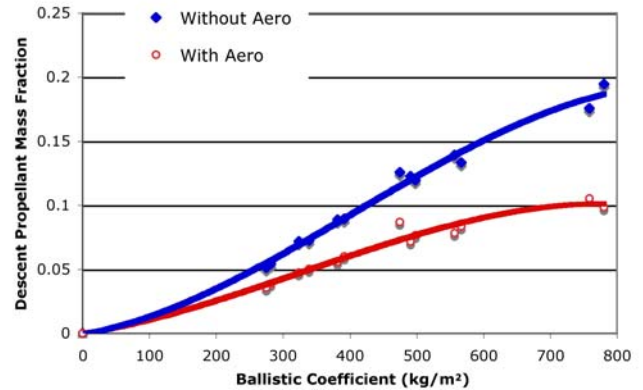

Figure 1. Impact of Neglecting Aerodynamic Effects of Supersonic Retropropulsion on Descent Propellant Mass Fraction for a Configuration with Nozzles Located at the Vehicle Periphery

As discussed in Section 4, a configuration with retronozzles located at the periphery of the forebody is most effective for supersonic deceleration, increasing the total axial force on the entry vehicle by approximately a factor of 2 for a thrust coefficient near 1.0 [15]. Experimentally observed aerodynamic, aerothermodynamic, and configuration trends for systems utilizing supersonic retropropulsion are discussed in detail in Sections 3, 4, and 5.

The ability of retropropulsion to substantially alter the aerodynamic characteristics of an entry vehicle at supersonic velocities with a T/W consistent or even lower than required for past missions suggests the possibility of using retropropulsion to close the supersonic deceleration technology gap. The use of supersonic retropropulsion as a supersonic decelerator for high mass EDL missions will depend on the relative degree of difficulty to develop this technology as compared to other candidate decelerators.rators

3 GENERAL FLOW CHARACTERISTICS

The effects of supersonic nozzle flow exhausting from a blunt body opposing a supersonic or hypersonic freestream result in an interaction between the nozzle flow and the detached bow shock. Resultant flowfields surrounding blunt bodies with no retropropulsion, configurations with nozzle flow from the center of the vehicle forebody, and configurations with nozzle flow from the periphery of the

vehicle forebody each exhibit fundamentally different behavior. Flowfield geometry and stability are highly dependent on the nozzle location (central vs. peripheral) and the relative strength of the nozzle flow, often given as a function of the ratio of the total pressure of the jet flow to the total pressure of the freestream. For a fixed set of freestream conditions, namely freestream total pressure, the strength of the nozzle flow as compared to the freestream can be characterized by the propulsive effort alone, or thrust coefficient. To compare resultant effects at different freestream conditions, the total pressure ratio must be used; the thrust coefficient is used for convenience when the freestream conditions are fixed.

Blunt Bodies without Retropropulsion

As a blunt entry body travels through the atmosphere of a planet, the flowfield surrounding the vehicle evolves as it descends to the surface. Peak heating generally occurs near the end of the transitional flow regime, where the atmosphere has become denser, and collisions between the incoming and reflected atmospheric molecules can no longer be ignored [16]. By the time aerodynamic drag has decelerated the vehicle to supersonic speeds, the vehicle is well into the continuum flow regime where the Navier-Stokes equations are valid [16]. In the late transitional to continuum flow regimes, the flow over a blunt entry vehicle is characterized by a strong detached bow shock [17].

The primary flow features are also strong functions of the sonic line location between the bow shock and the body. If the sonic line is over the nose of the vehicle, the pressure distribution downstream of the sonic line is flat from the nose to the shoulder [16]. Newtonian methods are adequate to predict the pressure distribution, and subsequently the static aerodynamic coefficients in this case. However, if the sonic line is nearer the shoulder of the vehicle, the pressure distribution is monotonically decreasing away from the nose, and Newtonian methods will both over and under-predict the pressure distributions at the nose and shoulder, respectively [16]. Where the sonic line remains close to the boundary layer over most of the vehicle, the pressure distributions near the shoulder of the vehicle can change rapidly. In this case, these changes in the pressure distribution, coupled with the largest moment arm being from the shoulder, can cause significant variation in the static aerodynamic moment coefficient [16].

For blunt bodies without retropropulsion, flow separation typically occurs near the shoulder, where the flow turning angle is large. The region of high pressure behind the vehicle creates recirculation regions composed of the separated flow. The extent of the separation decreases with decreasing Reynolds number [16].

Central Retropropulsion Configurations

The majority of the literature focuses on retropropulsion configurations where either a single nozzle or small cluster of nozzles is located along the body centerline on the forebody. An example of a central retropropulsion configuration with a single nozzle is shown in Figure 2.

Figure 2. Example of a Central Retropropulsion Configuration with a Single Nozzle

Figure 3 (adapted from [18]) illustrates the characteristic flowfield features for a central configuration and the complexity of the interaction between the nozzle flow and the freestream shock structure. The primary flow structures are the bow shock, free stagnation point, jet terminal shock, and the recirculation regions [18]. The location, degree of formation, and stability of these features are a strong function of the ratio of jet total pressure to freestream total pressure. This total pressure ratio is often represented by thrust coefficient, assuming a fixed freestream stagnation pressure for a given test condition [18].
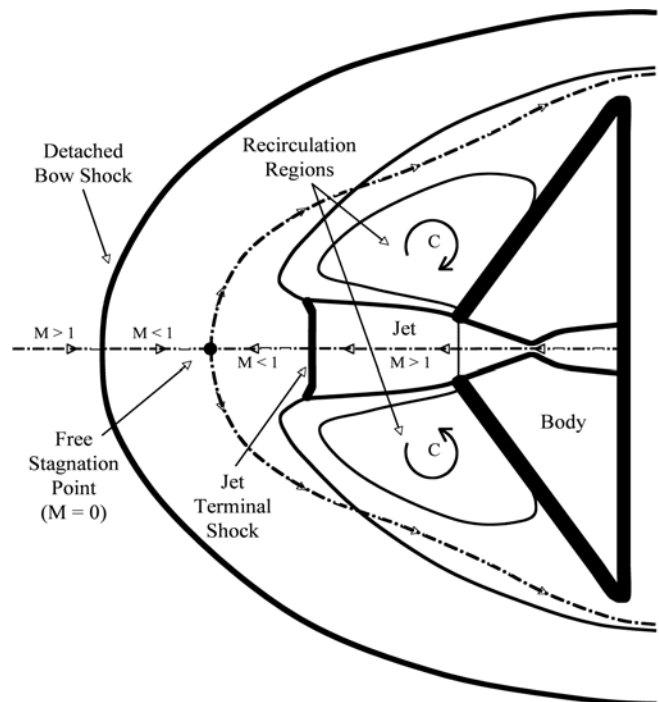

Figure 3. Characteristic Flowfield (adapted from [18])

The entire flowfield structure is dependent on the formation of the stagnation point. The freestream must decelerate to zero velocity, first from supersonic to subsonic through a shock wave, then from subsonic to zero velocity at the stagnation point [18]. The nozzle flow undergoes a similar

deceleration through mixing, viscous dissipation, or a normal shock, depending on the strength of the nozzle exhaust flow. The stagnation region consists of two supersonic regions, the freestream and nozzle flow, and a subsonic region divided by a contact discontinuity, the stagnation point [19].

The interaction of the jet with the opposing supersonic freestream in central configurations has been observed to cause the flowfield to transition from stable to highly unstable and back to stable as the total pressure ratio increases [18],[20]. This behavior is shown by Mach number contours in Figure 4 [21]. A stable flowfield occurs when the bow shock is close to the body, and the jet flow does not penetrate the bow shock; in this case, the flowfield structure is not oscillating. An unstable flowfield occurs when the jet shock penetrates the bow shock and the total shock displacement is significantly greater than the displacement characteristic of the stable condition. This displacement increases to a maximum with increasing total pressure ration and then collapses back to a displacement similar to the original stable case [15],[19],[21].
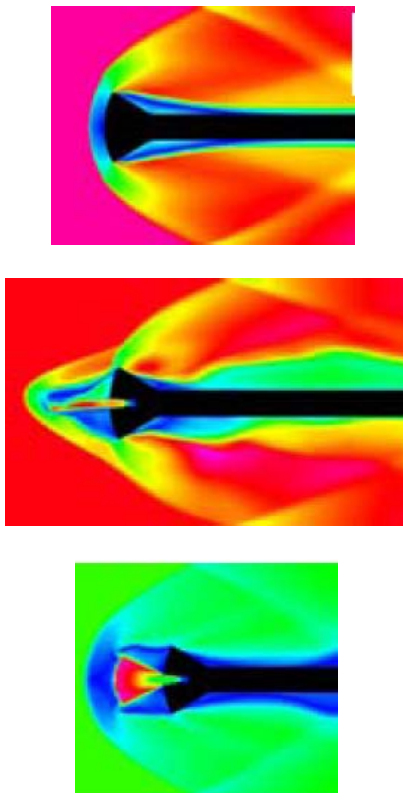

Figure 4. Stability Transitions With Increasing Jet Flow for Central Configurations (CFD Solutions) [21]

This stability transition phenomenon is not thoroughly understood. However, the boundaries of the different flow regimes can be partially correlated to changes in relative mass flow and by increases in the ratio of jet total pressure to freestream total pressure. At low flow rates (low total pressure ratios), the exhaust flow is retained within the

boundary layer and lacks sufficient momentum to disturb the bow shock [19].

As the nozzle flow rate increases, the nozzle flow cannot be contained within the boundary layer and begins to interact with the bow shock. The shock standoff distance increases proportionally with increasing nozzle flow until reaching a maximum displacement on the order of 6-7 body diameters [20]. In this unstable regime, the dissipative mechanism that allows the jet stagnation pressure to equal the freestream stagnation pressure at the interface is viscosity. These viscous losses require a greater jet length for the pressure adjustment to occur [20].

As the flow rate increases further, the shock standoff distance rapidly decreases, and the entire flow structure collapses back to a stable condition. In this case, the dissipative mechanism is a terminal shock, with the resulting subsonic jet flow stable enough to form a clear stagnation point [19],[20]. The nozzle exit Mach number determines the expansion condition of the jet flow (underexpanded or overexpanded), hence determining which of the dissipative mechanisms is dominant. Mixing and viscous dissipation is typically associated with underexpanded jet flow, and shock dissipation is common of overexpanded jet flow [20],[22]. This transition from a stable flowfield to an unstable flowfield occurs at lower thrust coefficients for smaller nozzles and at larger coefficients for larger nozzles, indicating dependence on the ratio of nozzle exit diameter to body diameter [23].

In a case with multiple nozzles arranged about the body axis of symmetry close to the vehicle centerline, Peterson and McKenzie [24] observed the same stability transitions as seen for the single, centrally-located nozzle. At low flow rates, the nozzle flows do not interact with one another. However, as the flow rate increases, the individual jet flows begin to coalesce into a single jet flow and interact with the bow shock, resulting in large shock displacement.

Peripheral Retropropulsion Configurations

In contrast to the central retropropulsion configuration, few references are available on retropropulsion configurations with nozzles at the periphery of the forebody. The primary documented investigations on peripheral configurations are experimental work by Jarvinen and Adams [15],[25] and Keyes and Hefner [26].

In a peripheral retropropulsion configuration, such as the one shown in Figure 5, the nozzle flow interacts with the bow shock differently than in a central configuration. The flow from each nozzle is swept away from the forebody and, at low flow rates, diffused into the opposing freestream by mixing [15]. Accordingly, flowfields for peripheral configurations do not have the large recirculation regions over the body surface characteristic of central configurations. Rather, the flowfield has a uniform region of high pressure inboard of the nozzles, resulting from the

lack of disturbance to the portion of the bow shock nearest the nose of the blunt body. A smaller flow turning angle is required than for a central configuration, preventing the nozzle flow from disturbing the center of the bow shock.

Figure 5. Example of a Peripheral Retropropulsion Configuration

As the thrust coefficient increases, the bow shock standoff distance increases. With additional increases, the resultant flowfield becomes increasingly unsteady as the jets begin to disturb the bow shock [18]. The nozzle flow now diffuses through a terminal shock instead of mixing with the freestream [15]. Both Jarvinen and Adams [15],[25] and Keyes and Hefner [26] observed local instabilities affecting the slope of the bow shock as the total thrust coefficient increased beyond approximately 3.0. Despite local instabilities causing rippling of the bow shock, the sharp increase in standoff distance and dissolution of the bow shock seen with the central nozzle configuration have not been observed with the peripheral nozzle configuration. Future work will be required to fully characterize the flowfield stability of configurations with peripheral nozzles.

4 AERODYNAMIC CHARACTERISTICS

The effects of supersonic retropropulsion flowfields on the aerodynamics of a blunt-bodied entry vehicle influence the configurations of retropropulsion desirable for EDL applications as a supersonic decelerator. The configuration of nozzles on the forebody and the ratio of the jet total pressure to the freestream total pressure govern the aerodynamic characteristics and static stability. Central and peripheral retropropulsion configurations exhibit fundamentally different flow behavior, resulting in contrasting aerodynamic effects.

Central Retropropulsion Configurations

A substantial number of experiments were done from the late 1950s through the early 1970s on the aerodynamic effects of a centrally-located retronozzle for EDL applications. For blunt cones, hemispheres, and other bodies of revolution, at Mach numbers from 1.05 to 9, the results of these experiments indicate that the central retropropulsion configuration is unfavorable for use as a supersonic decelerator from an aerodynamic standpoint. References [15], [18]–[25], and [27]–[35] are all experimental investigations of central retropropulsion configurations.

With increasing thrust coefficient, the aerodynamic drag coefficient decreases rapidly to a minimum value of approximately 10% of the no-jet value and then remains constant at this minimum value. For thrust coefficients above approximately 1.5, the total axial force coefficient is dominated by the contribution from the thrust coefficient. Extensive flow separation and the associated low surface pressures cause the total axial force coefficient to be higher than the no jet case at thrust coefficients greater than approximately 0.7. These effects are shown in Figure 6 (adapted from [23]).
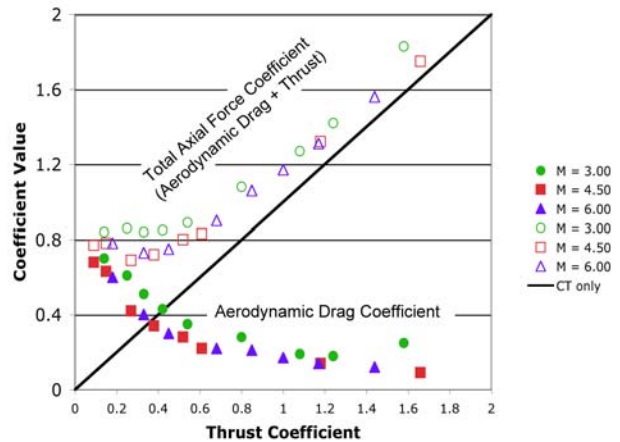

Figure 6. Aerodynamic Drag Coefficient Variation with Increasing Thrust Coefficient (adapted from [23])

With flow from a central nozzle, the high stagnation pressure present in the no jet case is greatly reduced. The nozzle flow perturbs the bow shock to become more oblique than normal. This reduction in shock strength leads to a reduction in surface pressure, and subsequently aerodynamic drag [27]. The degree of these surface pressure reductions tends to increase as the freestream Mach number increases [23].

At thrust coefficients greater than approximately 0.2, the nozzle flow cannot be contained within the boundary layer, and a sharp flow turning angle causes the boundary layer to separate on both sides of the jet on the forebody. Strong recirculation regions form on both sides of the nozzle flow, moving the flow within the shock layer towards the vehicle's shoulder. Flow reattachment begins near a thrust coefficient of 2, and by higher thrust coefficients (at approximately $C_T = 6$), the base pressure of the body equals the forebody pressure, enveloping the body in a constant pressure region similar to wake flow [15],[23]. Little variation in the surface pressure is seen between different blunt body geometries, indicating a relative independence of aeroshell cone angle on the drag reduction effects of central retropropulsion configurations.

Romeo and Sterrett [20] examined flowfield stability for a centrally-located jet over angles of attack from 0° to 35°. Beyond very small angles of attack (greater than 2°), the structure of the flowfield breaks down for total pressure ratios (or thrust coefficients) corresponding to the case where the jet penetrates the bow shock and resulting standoff distance is large.

The pitching moment slopes for increasing thrust coefficients at freestream Mach numbers of 1.05 and 2.0 are shown in Figure 7 [15]. The data were taken over angles of attack from -6° to +6°. For the central nozzle configuration, the pitching moment coefficient for a given thrust coefficient is nearly linear with variation in angle of attack. Subsequently, angle of attack variation is not included in Figure 7. The pitching moment slope becomes increasingly negative as the thrust coefficient increases to 1, then becomes less negative with additional increases in thrust coefficient. The pitching moment slope is always negative, indicating that the entry body is statically stable. This static stability is observed even in cases where the flowfield itself may be unstable.
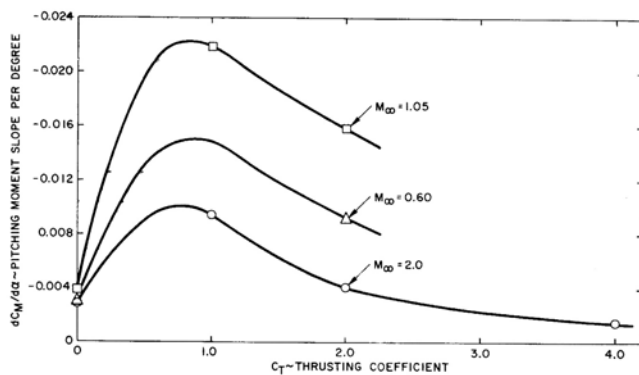

Figure 7. Variation of Pitching Moment Slope with Thrust Coefficient [15]

The severe reduction in aerodynamic drag contribution to the total axial force coefficient by centrally-located nozzle configurations is a drawback in this technology's application for supersonic deceleration. The flowfield stability transitions and observed flow unsteadiness over most freestream Mach numbers and thrust coefficients investigated are additional complications to the implementation of this configuration into an EDL architecture.

Peripheral Retropropulsion Configurations

From the standpoint of aerodynamic drag benefit, configurations where the nozzles are at the periphery of the forebody of a blunt entry vehicle are promising. Both Jarvinen and Adams [15],[25] and Keyes and Hefner [26] experimentally observed augmentation of the total axial force coefficient at modest nozzle flow rates, a significant contrast to the reduction seen for configurations with retropropulsion along the body centerline. Experimental data has been taken at freestream Mach numbers of 1.05,

1.50, 2.0, and 6.0, using 60° sphere-cones, using air for the freestream and nozzle flow.

The lack of disruption of the center of the bow shock by the peripheral nozzle flow causes a region of high pressure to remain over portions of the aeroshell inboard of the nozzles, preserving the aerodynamic drag of the aeroshell [26]. The bow shock remains sufficiently undisturbed and close to the body for total thrust coefficients below 5.0 [15].

Experimental work by Jarvinen and Adams [15],[25] demonstrated a range of thrust coefficients over which a three-nozzle configuration (see Figure 5) provides substantially more total axial force than a single, centrally-located nozzle at the same total thrust coefficient. The comparison of total axial force coefficient between a peripheral nozzle configuration and a central nozzle configuration at the same conditions is shown in Figure 8 [15].
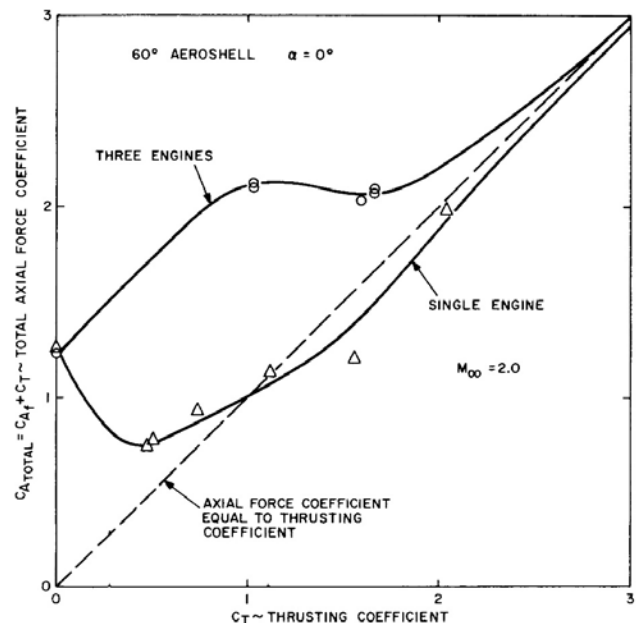

Figure 7. Comparison of Total Axial Force Coefficient for Peripheral and Central Configurations [15]

A configuration with three nozzles at the body periphery outperforms the configuration with a single central nozzle for thrust coefficients up to 2. At thrust coefficients above 2, the total axial force coefficients for both configurations are nearly equal to the thrust coefficient alone, given by the dashed line in Figure 8 [15].

At lower thrust coefficients, the nozzle flow only mildly disturbs the bow shock at the edges. This perturbation acts to flatten the bow shock at the edges, causing the flowfield to effectively see a larger blunt body. At higher thrust coefficients, the nozzle flow penetrates the bow shock, and the high pressure region inboard of the nozzles disappears as the bow shock weakens [15],[26].

The augmentation of the total axial force coefficient is dependent on freestream Mach number. The maximum increase in total axial force coefficient, observed near a thrust coefficient of 1.0, increases over the freestream Mach numbers tested, likely due to the increasing strength of the bow shock [15]. In these cases, an axial force augmentation approximately equal to the thrust force is possible. Surface pressure data confirms that the aeroshell surface is covered with a nearly uniform region of high pressure, and this surface pressure is highest at total thrust coefficients near 1.0 [15].

Variation of angle of attack, from -6º to +6º, showed little effect on the forebody axial force coefficient for freestream Mach numbers 1.05, 1.50, and 2.0 with thrust coefficients from 0 to 1.9 [15]. In contrast to the central nozzle configuration, the pitching moment coefficient exhibits nonlinear behavior, as shown in Figure 9 [15]. For a thrust coefficient of 1.04, a transonic condition, the body is statically unstable at angles of attack between -2º and -8º. The varying nonlinearity and indiscernible dependence on thrust coefficient causes difficulty in determining a trend in static stability with increasing thrust coefficient with the limited data available for the peripheral configuration.
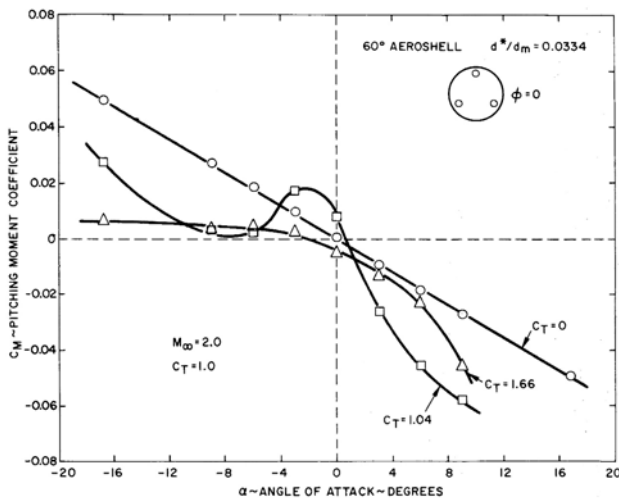

Figure 8. Variation of Pitching Moment Coefficient with Thrust Coefficient and Angle of Attack [15]

The marked increase in the total axial force coefficient for low to modest thrust coefficients make peripheral retropropulsion configurations favorable for EDL applications as a supersonic decelerator. The maximum augmentation in total axial force occurs at total pressure ratios (equivalently low thrust coefficients) typical of stable flowfields. However, the existing experimental database for peripheral configurations is limited, suggesting a need to expand the database to additional configurations and conditions for accurate comparison between peripheral retropropulsion configurations and alternative supersonic decelerator technologies.

Differential Throttling Effects

Jarvinen and Adams [15],[25] also explored drag modulation capability by throttling combinations of three engines of a peripheral retropropulsion configuration. The amount of variation in total axial force coefficient between throttled and unthrottled conditions was observed to increase with increasing freestream Mach number. At a freestream Mach number of 1.05, little variation between the no throttling case and cases where one engine was throttled down by 50% and 75% was observed at thrust coefficients below 3.0. However, in a Mach 2.0 freestream, significant variation between the two cases was observed at total thrust coefficients above 1.0.

Similar departures were observed under the same conditions for cases where two of the three engines were throttled down [15]. In the $M_\infty = 1.05$ case, with one engine throttled down by 50% and the total thrust coefficient increased from 0.5 to 3.0, the forebody drag coefficient decreased from 0.8 to approximately zero. At the same freestream conditions, with two engines throttled down and the thrust coefficient increased from 0.5 to 3.0, the forebody drag coefficient decreased from 0.8 to approximately -0.4. In the $M_\infty = 2.0$ case, with one engine throttled down and the thrust coefficient increased from 0.5 to 3.0, the forebody drag coefficient decreased from 1.2 to approximately -0.1. In the $M_\infty = 2.0$ case, with two engines throttled down and the thrust coefficient increased from 0.5 to 3.0, the forebody drag coefficient decreased from 1.2 to approximately 0.1. Jarvinen and Adams [15] concluded that as freestream Mach number increased, the same degree of forebody drag coefficient modulation could be realized with decreasing thrust coefficients.

Throttling combinations of engines at the body periphery also produced alterations in the static stability of the vehicle [15]. The total pitching moment on the body is the sum of the pitching moment due to surface pressure forces and the pitching moment induced by imbalances in thrust. In cases where the blunt body was oriented at a positive angle of attack, throttling down engines on the leeward side of the forebody induced a nose-down pitching moment. In the same orientation, throttling down engines on the windward size of the forebody induced a nose-up pitching moment.

These induced pitching moments can be attributed to the asymmetry of the detached bow shock, a condition arising from the non-uniform engine thrust and resulting total axial force changes at throttled conditions. Schlieren images [15] show an increase in standoff distance and an increase in the obliqueness of the local section of the bow shock in the region of the unthrottled nozzle flow. The decrease in shock strength with the increase in obliqueness support the conclusion that the reduction in axial force coefficient with increasing thrust coefficient is strongly dependent on changes to the surface pressure distribution caused by throttling. The effectiveness of throttling in controlling pitching moment, defined as the ratio of change in pitching

moment measured experimentally to the change in pitching moment due solely to an imbalance in engine thrust, was observed to be reduced by 20% at supersonic freestream conditions as compared to throttling efficiency at subsonic velocities. Jarvinen and Adams [15],[25] attributed this reduction in throttling effectiveness to the effect of supersonic freestream conditions on the total axial force coefficient.

5 AEROTHERMODYNAMIC CHARACTERISTICS

The effects of supersonic retropropulsion on heat transfer to an entry vehicle are significant, particularly if the nozzle flow is composed of combustion products. At supersonic speeds, the primary heating contribution is not likely aerodynamic, but from exhausting high enthalpy combustion products into the region between the bow shock and the body. Instances of increased total heat transfer can be twice as high as for cases with no retropropulsion. The aerothermodynamic effects of retropropulsion have only been investigated for central retropropulsion configurations. Similar to the trends in aerodynamics and stability, the aerothermal effects are highly dependent on the ratio of jet total pressure to freestream total pressure. These effects also depend on the gas species involved. At low flow rates, the order of the heat transfer to the body is of the order of the heat capacity of the nozzle exhaust, defined as the amount of heat the gas between the bow shock and the body can absorb in having its temperature raised from the temperature of the nozzle exhaust to the freestream stagnation temperature [35]. Increases in heat transfer rate are significantly larger for injected gases with lighter molecular weights [19],[36].

Desirable diffusive properties of the nozzle flow, such as small Schmidt number and large Prandtl number, are secondary in importance to the thermal properties discussed above [36]. The Schmidt number and Prandtl number are dimensionless quantities relating momentum to mass transfer and heat transfer, respectively. A small Schmidt number means that the mass diffuses quickly, as compared to the velocity. A large Prandtl number means heat diffuses slowly, as compared to the velocity. These characteristics allow for the maximum amount of heat, from the freestream and the nozzle exhaust, to be carried away from the body, and hence are desirable properties of the nozzle exhaust flow [36].

Combustion effects, observed by Barber [19],[34] through hydrogen-air combustion during boundary layer injection, appear to be significant contributors to the total enthalpy of the flowfield. Heat transfer generally decreases for injected noncombustible gases and increases rapidly for combustible gases, with the combustion process significantly increasing the enthalpy of the nozzle flow [19],[34]. For the thrust magnitudes required for human Mars exploration, the propulsion system likely to be selected for the entry vehicle will be LOX/methane or LOX/hydrogen, resulting in

significant heating contributions from combustion products [11],[12].

An opposite effect, reductions in the heat transfer rate, has also been observed at supersonic test conditions where the exhaust gases are cold. Reductions in heat flux in the stagnation region can be greater than 50%, as observed by Barber [19],[34], Daso [21], Hayashi, et al. [37],[38], and Stalder and Inouye [39]. This effect is illustrated in Figure 10 for an air freestream at mach 3.98 with nitrogen nozzle exhaust, showing a decrease in surface heat flux for a given position away from the body nose in the stagnation region as the total pressure ratio increases from 0 (no jet) to 0.80 (maximum jet pressure ratio tested in this case) [37].
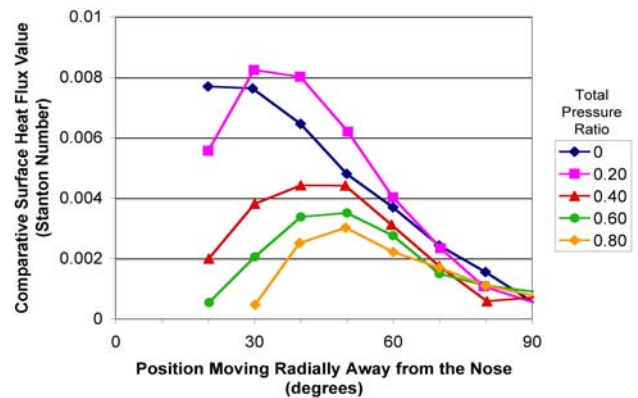

Figure 10. Heat Flux Distribution for Varying Total Pressure Ratios [37]

Stanton number was used to compare each heat flux distribution because the test conditions were slightly different in each case. Stanton number is a dimensionless quantity directly proportional to heat transfer. It was also observed that heavier gases require larger mass flows than the lighter gases to achieve the same reductions in heat flux [40].

Experimental work by Grenich [41] examined the case where the exhaust gases have only about 20% of the total enthalpy of the freestream, as would be typical for the use of a coolant gas to reduce heat transfer to an entry body at hypersonic velocities. In this case, the heat transfer to the body is significantly reduced as the body is blanketed with the cooler gas being swept back along the body from a nozzle aligned with the body centerline [41]. These cooler gases form a region of recirculation, blocking the higher enthalpy freestream gases from directly contacting the body surface [38]. Injecting a gas with high specific heat into the boundary layer via retropropulsion effectively increases the thickness of the boundary layer, reducing convective heat transfer to the body surface. This effect can be difficult to achieve and depends on how the injected gas diffuses through the boundary layer [36]. When the injected gas had gained sufficient momentum to extend beyond the boundary layer, a reduction in surface heat transfer was no longer observed.

Barber [19] and Warren [35] observed cases where the heat transfer in the stagnation region of the body was reduced, but the heat transfer over the entire body was greater than in the case where no retropropulsion was used. In these cases, the stagnation region of the body is cooled locally, but downstream of the nose, the flow reattaches to the body, creating a stagnation ring, or annulus region. The pressure is greatly reduced in this dead-air region, resulting in lower surface heat flux [35]. At the reattachment point, however, the pressure is higher than the case of no retropropulsion [35],[42].

Experimental data on the aerothemodynamic effects of supersonic retropropulsion is limited in scope and remains an area of active research. No data exists for multiple nozzle configurations, particularly those discussed in the prior sections as promising configurations for high ballistic coefficient entry systems. Finley [18] argues that the study by Warren [35] does not have high enough flow rates to have stable flowfields, potentially limiting the applicability of Warren's results. The impact of combustion products in the exhaust flow has only been observed for exhaust contained within the boundary layer, and the enthalpy added to the stagnation region by the combustion process may prove to be a detrimental effect of supersonic retropropulsion systems.

6 EXPERIMENTAL SUMMARY

The focused technology development program for planetary exploration in the 1960s and early 1970s matured supersonic retropropulsion close to its current level of development through a number of experimental investigations. The original intent of these experiments was to explore supersonic retropropulsion to understand drag effects potentially advantageous to EDL. Scaling parameters were developed to accurately simulate the larger chemical bipropellant propulsion systems visualized for conceptual Mars landers using subscale models. To date, only monopropellant descent propulsion systems have been flown. No work has been found in support of missions to destinations other than Mars.

Simulation Parameters for Similarity and Scaling

Pindzola [43] developed methods for simulating nozzle flow using ground facilities and selecting geometries and test conditions to account for differences in chemical species properties between models and full scale. Primary jet flow parameters are governed by relations to nozzle mass flow, enthalpy, and momentum. The methods of simulating retropropulsion jets using cold gas and hot gas are used in much of the experimental work on aerodynamics and aerothermodynamics discussed in Sections 3-5.

Jarvinen and Adams [15],[25][31] extended Pindzola's methods for accurately simulating jet flows in a wind tunnel to the retrorocket exhaust of a conceptual Mars lander. The

freestream Mach number, thrust coefficient, plume sensitivity parameter, and engine scaling parameter are the scaling parameters matched for proper simulation of retrorocket flow at subscale in a wind tunnel.

The nozzle exhaust flow is simulated by matching the ratio of pressure at the nozzle exit to the ambient pressure and the pressure sensitivity of the exhaust flow with respect to the flow direction, given by Equation 2, where P is the pressure and ν is the flow direction at the nozzle exit plane. Equation 2 is also known as the plume sensitivity parameter [15],[43].

$$\frac{1}{P}\frac{dP}{d\nu} \tag{2}$$

The thrust coefficient, given previously by Equation 1, is the primary parameter governing the interaction between nozzle flow and an opposing supersonic freestream. The thrust coefficient can be rewritten in terms of both freestream and nozzle flow parameters, shown by Equation 3 [15] where A_B is the model base area, A_e is the nozzle exit area, and γ_∞ and γ_e are the ratio of specific heats of the freestream and at the nozzle exit, respectively.

$$C_T = \frac{2}{\gamma_\infty M_\infty^2}\frac{P_e}{P_\infty}\frac{A_e}{A_B}\left(1+\gamma_e M_e^2\right) \tag{3}$$

Rearranging Equation 3 to have all freestream parameters except γ_∞ on the left-hand side and all nozzle flow parameters on the right-hand side gives the engine scaling parameter, defined by Equation 4 [15].

$$\frac{\gamma_\infty A_B}{2A_e\left(1+\gamma_e M_e^2\right)} \tag{4}$$

Existing Experimental Database

While numerous wind tunnel tests were conducted, the scope of the work was limited in terms of freestream conditions, retropropulsion conditions, and body geometries. The majority of past efforts focused on blunt bodies with a single, centrally-located nozzle – a configuration which does not appear to be favorable for supersonic deceleration applications due to its significant reductions in the aerodynamic drag of the blunt body. Only three investigations have used multiple nozzles (References [15],[24],[25]). An additional limitation of the existing data is the use of compressed air, nitrogen, hydrogen, or helium in all test cases for the nozzle exhaust. No experimental data exists for supersonic retropropulsion simulation using combustion nozzles, possibly due to test scale and the complexity of combustion nozzle systems. The primary goal of most of these investigates was to explore potential reductions in heat transfer, not deceleration. The flow conditions in the existing experimental database are summarized in Table 2.

Table 2. Existing Experimental Database

Available Central Nozzle Configuration Data

Relevance	Freestream Mach	Freestream	Jet	References
Static Aerodynamics	1.05 - 6.0, 20-21	Air	Air, Helium	[15],[18]-[21],[23]-[25],[27]-[29],[31]-[35],[37],[39]-[41],[44]
Flowfield Stability	1.05 - 6.0	Air	Air, Helium	[15],[18],[23]-[25],[27],[37]
Flowfield Geometry	1.05 - 8.0	Air	Air, Helium	[15],[18]-[21],[23]-[25],[28]-[29],[31]-[34],[40]
Effect of Nozzle Geometry	1.05 - 6.0, 20-21	Air	Air, Helium	[15],[18],[20]-[21],[25],[31],[39],[41]
Angle of Attack Variation	1.05 - 6.0	Air	Air, Helium	[15],[20],[23]-[25]
Aerothermodynamics	2.0, 6.0-8.0, 20-21	Air	Air	[19],[21],[34]-[42],[45]
Systems Level Implications	1.05 - 6.0	Air	Air	[15],[20],[25],[27],[41]

Available Peripheral Nozzle Configuration Data

Relevance	Freestream Mach	Freestream	Jet	References
Static Aerodynamics	1.05 - 6.0	Air	Air	[15],[25]-[26]
Flowfield Stability	1.05 - 2.0	Air	Air	[15],[25]
Flowfield Geometry	1.05 - 2.0	Air	Air	[15],[25]-[26]
Effect of Nozzle Geometry	1.05 - 2.0	Air	Air	[15],[25]
Angle of Attack Variation	1.05 - 2.0	Air	Air	[15],[25]
Aerothermodynamics	None	N/A	N/A	N/A
Systems Level Implications	1.05 - 2.0	Air	Air	[15],[25]-[26]

This experimental database will need to be expanded to include additional retropropulsion configurations, body geometries, exhaust and freestream species, combustion retropropulsion, and a broader range of flow conditions. Slender body geometries such as biconics and ellipsleds are candidates for human Mars architectures, and no data exists to validate computational simulation of supersonic retropropulsion systems derived for these geometries. As the work by Peterson and McKenzie [24] is the only configuration of multiple nozzles not located on the body periphery, the answer to how far apart multiple nozzles need to be spaced to prevent an interaction between the exhaust jets remains unknown.

7 COMPUTATIONAL ANALYSES

Few papers have been published on the computational modeling and analysis of supersonic retropropulsion. Recent work has focused on drag reduction for slender body vehicles, not drag augmentation for blunt bodies, and the effects of high temperature plasma jets on the body aerodynamics [44],[45]. However, the similarities in flowfield interactions between these applications and supersonic retropropulsion for EDL have been useful in extending computational approaches.

Computational solutions of supersonic retropropulsion systems will need to capture as many of the following characteristics as possible:

(1) Flow features such as strong shocks, shock/boundary layer interactions, shock-shock interactions, and recirculation.

(2) Viscous effects within the shock layer.

(3) Relevant equilibrium and nonequilibrium chemistry.

(4) Diffusion and transport properties of the exhaust flow.

(5) Radiative energy transfer in the flow, if necessary.

Additionally, oscillatory behavior, characteristic of even stable flowfields, makes starting solutions and defining convergence difficult. Despite these challenges, several studies [21],[37],[44],[45] have shown varying degrees of success in modeling the aerothermodynamics of single nozzle configurations.

Daso [21] completed pre-test computational fluid dynamics (CFD) analysis with a 2.6% scale model of the Apollo capsule with and without retropropulsion effects. The CFD analysis was attempting to predict the aerodynamic and aerothermodynamic effects of a centrally-located nozzle in air at freestream Mach numbers of 3.48 and 4.0. Both the

pre-test computational simulations and associated experiment used compressed air for the nozzle exhaust [21]. While little attention is presented on the details of the CFD analysis, the use of a 3-D structured grid Navier-Stokes solver predicted the transitions in flow stability and captured the general aerothermodynamic trends. The characteristic unsteadiness and oscillatory behavior of the flowfields with retropropulsion resulted in asymmetric flowfield geometries.

Fomin and Maslov [44] performed numerical simulations in support of experimental work on the blunt-body pressure effects of a high temperature plasma jet at freestream Mach numbers of 2.0, 2.5, and 4.0. Composition of the freestream was air, and the plasma jet was nitrogen gas at 5000 K. The experimental results were compared against an Euler CFD analysis in an effort to understand the separation existing between fluid dynamics and the thermal processes in a supersonic freestream-propulsion interaction. The Euler solver was able to capture the reduction in body surface pressures caused by transition to unstable flow and jet penetration of the bow shock. The relatively good agreement seen between the Euler solutions and the experimental plasma jet work suggests much of the interactions at lower supersonic Mach numbers resemble retropropulsion gas dynamics, a result promising for future work with combusting retropropulsion effects [44]. Additional work from the same authors has been reported to have had success with modeling supersonic retropropulsion in the form of plasma jets, using the assumption of a perfect gas with constant specific heats [45].

Hayashi, et al. [37] solved the axisymmetric Navier-Stokes equations to predict reductions in aerothermal heating in the stagnation region of a hemisphere at a freestream Mach number of 3.96. Freestream composition was air, and the nozzle exhaust was nitrogen gas at 300 K. The CFD results showed good agreement with experiment, particularly in the ability to capture the recirculation regions about a centrally-located jet. The strength of the recirculation regions was slightly higher than observed experimentally, resulting in more efficient heat flux reduction in the CFD solution than observed in the experiment.

Computational simulation of the interactions between retronozzles and supersonic freestreams is the next phase of investigation required to mature supersonic retropropulsion from a potentially feasible concept to a useful EDL technology. The ability of preliminary CFD investigations to capture trends in surface pressure, flowfield geometry, and patterns of heat flux, despite unsteadiness and oscillatory behavior, is encouraging for the continued development of approaches for high-fidelity computational modeling. While these preliminary efforts are good first steps in developing computational capability, much of the physics relevant to the behavior of supersonic retropropulsion is coupled and viscous in nature, unable to be fully captured at this point. Flow separation, recirculation, boundary layer transition, and oscillation of the position of primary flow features such as the detached bow shock, free stagnation point, and jet flow boundary are characteristic of supersonic retropropulsion flowfields and have only been captured under a very limited range of conditions.

8 CONCLUDING REMARKS

Interactions between retropropulsion exhaust and blunt body aerodynamics have been investigated since the early 1950s. Extensive wind tunnel experiments in the 1960s and early 1970s developed the technology to near the level of maturity it has today. Experimental results consistently show, for low thrust coefficients, significant axial force augmentation (aerodynamic drag and thrust) for peripheral retropropulsion configurations and little or no augmentation of axial force beyond that provided by the retrorocket thrust for configurations with the nozzle located along the body centerline. This degree of aerodynamic interaction is strongly dependent on the location of the nozzles and the relative strength of the exhaust flow to the freestream. The primary parameter used to characterize the static aerodynamics and flowfield stability is the thrust coefficient, with the greatest degree of axial force augmentation for peripheral retropropulsion configurations occurring near a thrust coefficient of 1.0.

Despite the extensive focus on retropropulsion in the 1960s and early 1970s, significant limitations exist in the current experimental database. The most significant challenges in maturing supersonic retropropulsion are related to a lack of knowledge in the following areas:

(1) Configurations with nozzles at the body periphery and mid-to-high lift-to-drag ratio vehicle geometries.

(2) Aerothermal effects caused by exhausting combustion products into the shock layer.

(3) Uncertainties in scaling wind tunnel results to flight systems.

(4) Validated CFD approaches.

High mass, high ballistic coefficient requirements for Mars EDL, particularly for human exploration, are challenging the capabilities of heritage supersonic decelerators. Systems studies show vehicle T/W requirements similar to robotic Mars missions and performance requirements consistent with existing liquid bipropellant propulsion systems. Experimental work from the focused technology development program prior to the Viking missions and recent computational analyses suggest supersonic retropropulsion, in a configuration with the nozzles located at the periphery of the forebody, may be able to address this challenge, enabling the delivery of high-mass payloads to the surface of Mars.

REFERENCES

[1] R.D. Braun and R.M. Manning, "Mars Exploration Entry, Descent, and Landing Challenges," Journal of Spacecraft and Rockets, Vol. 44, No. 2, 310-323, March – April 2007.

[2] E. Love, "The Effect of Small Jet of Air Exhausting from the Nose of a Body of Revolution in Supersonic Flow", NACA RM L52I19a, November 1952.

[3] E. Love, "A Re-examination of the use of Simple Concepts for Predicting the Shape and Location of Detached Shock Waves," NACA TN-4170, 1957.

[4] E. Love, et al., "Experimental and Theoretical Studies of Axisymmetric Free Jets," NASA TR R-6, 1959.

[5] R. Huff and K. Abdalla, "Mixing Characteristics Downstream of Core Region of High-Temperature Axisymmetric Jets Exhausting into Transonic and Supersonic Streams," NASA TM X-151, March 1960.

[6] W. Moeckel, "Flow Separation Ahead of Blunt Bodies at Supersonic Speeds," NACA TN 2418, July 1951.

[7] W. Moeckel, "Flow Separation Ahead of a Blunt Axially Symmetric Body at Mach Numbers 1.76 to 2.10," NACA RM E51I25, December 1951.

[8] E. Love, M. Woodling, L. Lee, "Boundaries of Supersonic Axisymmetric Free Jets," NACA RM L56G18, October 1956.

[9] E. Love and C. Grigsby, "Some Studies of Axisymmetric Free Jets Exhausting From Sonic and Supersonic Nozzles into Still Air and Into Supersonic Freestreams," NACA RM L54L31, May 1955.

[10] B.G. Drake," Reference Mission Version 3.0: Addendum to the Human Exploration of Mars: The Reference Mission of the NASA Mars Exploration Study Team," NASA/SP-6107-ADD, June 1998.

[11] S.J. Hoffman (ed.) and D.I. Kaplan (ed.), "Human Exploration of Mars: The Reference Mission of the NASA Mars Exploration Study Team," NASA Johnson Space Center, July 1997.

[12] J. Christian, G. Wells, J. Lafleur, A. Verges, R. Braun, "Extension of Traditional Entry, Descent, and Landing Technologies for Human Mars Exploration," Journal of Spacecraft and Rockets, Vol. TBD, 2008.

[13] G. Wells, et al., "Entry, Descent, and Landing Challenges of Human Mars Exploration," 29th AAS Guidance and Control Conference, AAS 06-072, Breckenridge, Colorado, February 2006.

[14] L.G. Tanner, "Development and Characteristics of the Russian / American RD-180 Rocket Engine," AIAA Joint Propulsion Conference, Liquid Propulsion Short Course, Indianapolis, Indiana, July 2002.

[15] P. Jarvinen and R. Adams, "The Aerodynamic Characteristics of Large Angled Cones with Retrorockets," NASA Contract No. NAS 7-576, February 1970.

[16] P.A. Gnoffo, "Planetary-Entry Gas Dynamics," Annual Review of Fluid Mechanics, Vol. 31, 459-494, 1999.

[17] J. Campbell, "Supersonic Aerodynamic Characteristics and Shock Standoff Distances for Large-Angle Cones with and without Cylindrical Afterbodies," NASA TN D-5334, 1969.

[18] P.J. Finley, "The Flow of a Jet from a Body Opposing a Supersonic Free Stream," Journal of Fluid Mechanics, Vol. 26, No. 2, 337-368, October 1966.

[19] E.A. Barber, "An Experimental Investigation of Stagnation-Point Injection," Journal of Spacecraft and Rockets, Vol. 2., No. 5, 770-774, May 1965.

[20] D. Romeo and J. Sterrett, "Exploratory Investigation of the Effect of a Forward-Facing Jet on the Bow Shock of a Blunt Body in a Mach Number 6 Free Stream," NASA TN D-1605, February 1963

[21] E.O. Daso, V.E. Pritchett, and T.S. Wang, "The Dynamics of Shock Dispersion and Interactions in Supersonic Freestreams with Counterflowing Jets," 45th AIAA Aerospace Sciences Meeting, AIAA 2007-1423, Reno, Nevada, January 2007.

[22] A. Watt, "An Experimental Investigation of a Sonic Jet Directed Upstream Against a Uniform Supersonic Flow," Institute of Aerophysics, University of Toronto TN 7, January 1956.

[23] R. McGhee, "Effects of a Retronozzle Located at the Apex of a 140 Blunt Cone at Mach Numbers of 3.00, 4.50, and 6.00," NASA TN D-6002, January 1971.

[24] V. Peterson and R. McKenzie, "Effects of Simulated Retrorockets on the Aerodynamic Characteristics of a Body of Revolution at Mach Numbers from 0.25 to 1.90," NASA TN D-1300, May 1962.

[25] P. Jarvinen and R. Adams, "The Effects of Retrorockets on the Aerodynamic Characteristics of Conical Aeroshell Planetary Entry Vehicles," AIAA 70-219, *AIAA 8th Aerospace Sciences Meeting*, New York, New York, January 1970.

[26] J.W. Keyes and J.N. Hefner, "Effect of Forward Facing Jets on Aerodynamic Characteristics of Blunt Configurations at Mach 6," Journal of Spacecraft and Rockets, Vol. 4, No. 4, 533-534, April 1967.

[27] N. Charczenko and K. Hennessey, "Investigation of a Retrorocket Exhausting from the Nose of a Blunt Body into a Supersonic Free Stream," NASA TN D-751, September 1961.

[28] D. Romeo and J. Sterrett, "Flow Field for Sonic Jet Exhausting Counter to a Hypersonic Mainstream," AIAA Journal, Vol. 3 No. 3, 344-346, March 1965.

[29] R. Margason, "The Path of a Jet Directed at Large Angles to a Subsonic Free Stream," NASA TN D-4919, November 1968.

[30] A.F. Charwat and J. Allegre, "Interaction of a Supersonic Stream and a Transverse Supersonic Jet," AIAA Journal, Vol. 2, No. 11, 1965-1972, November 1964.

[31] P. Jarvinen and J. Hill, "Penetration of Retrorocket Exhausts into Subsonic Counterflows," Journal of Spacecraft and Rockets, Vol. 10, No. 1, 85-85, January 1973.

[32] L. Hayman and R. McDearmon, "Jet Effects on Cylindrical Afterbodies Housing Sonic and Supersonic Nozzles which Exhaust against a Supersonic Stream at Angles from 90 to 180 Degrees," NASA TN D-1016, March 1962.

[33] J. Baron and E. Alzner, "An Experimental Investigation of a Two Layer Inviscid Shock Cap due to Blunt Body Nose Injection," Journal of Fluid Mechanics, Vol. 15, No. 3, 442-448, March 1963.

[34] E.A. Barber, "An Experimental Investigation of Stagnation-Point Injection," *AIAA Conference on Physics of Entry into Planetary Atmospheres*, AIAA 1963-0433, Cambridge, Massachusetts, August 1963.

[35] C. Warren, "An Experimental Investigation of the Effect of Ejecting a Coolant Gas at the Nose of a Bluff Body," Journal of Fluid Mechanics, Vol. 2, No. 8, 400-417, 1960.

[36] L. Roberts, "Mass Transfer Cooling Near the Stagnation Point," NASA TR R-8, 1959.

[37] K. Hayashi, S. Aso, Y. Tani, "Numerical Study of Thermal Protection System by Opposing Jet," *43rd AIAA Aerospace Sciences Meeting*, AIAA 2005-0188, Reno, Nevada, January 2005.

[38] K. Hayashi and S. Aso, "Effect of Pressure Ratio on Aerodynamic Heating Reduction due to Opposing Jet," *33rd AIAA Fluid Dynamics Conference*, AIAA 2003-4041, Orlando, Florida, June 2003.

[39] J. Stalder and M. Inouye, "A Method of Reducing Heat Transfer to Blunt Bodies by Air Injection," NACA RM A56B27a, May 1956.

[40] J.E. Grimaud and L.C. McRee, "Experimental Data on Stagnation-Point Gas Injection Cooling on a Hemisphere-Cone in a Hypersonic Arc Tunnel," NASA TM X-983, July 1964.

[41] A.F. Grenich and W.C. Woods, "Flow Field Investigation of Atmospheric Braking for High Drag Vehicles with Forward Facing Jets," *AIAA 19th Aerospace Sciences Meeting*, AIAA 1981-0293, St. Louis, Missouri, January 1981.

[42] P. Chung, "Effect of Localized Mass Transfer Near the Stagnation Region of Blunt Bodies in Hypersonic Flight," NASA TN D-141, May 1960.

[43] M. Pindzola, "Jet Simulation in Ground Test Facilities," AGARDograph 79, November 1963.

[44] V.M. Fomin, A.A. Maslov, N.D. Malmuth, "Influence of a Counterflow Plasma Jet on Supersonic Blunt-Body Pressures," AIAA Journal, Vol. 40, No. 6, 1170-1177, June 2002.

[45] G.G. Chernyi, "Some Recent Results in Aerodynamic Applications of Flows with Localized Energy Addition," *9th International Space Planes and Hypersonic Systems and Technologies Conference*, AIAA 99-4819, Norfolk, Virginia, November 1999.

BIOGRAPHIES

Ashley M. Korzun is a graduate student in aerospace engineering at the Georgia Institute of Technology in the Space Systems Design Lab. Her research focuses on supersonic retropropulsion for planetary EDL applications, specifically at Mars, including systems-level analysis and the development of computational fluid dynamics approaches for modeling aerodynamics and aerothermodynamics. She is also the EDL lead for the Mars Gravity Biosatellite Program and an alum of the 2006 NASA Academy. She has a B.S. in Aerospace Engineering from the University of Maryland, College Park.

Juan R. Cruz is an aerospace engineer in the Atmospheric Flight and Entry Systems Branch at the NASA Langley Research Center. He has been involved with the development and qualification of the entry, descent, and landing system of several planetary exploration missions including the Mars Exploration Rovers and the Mars Science Laboratory. His current research focuses on the development of aerodynamic decelerators for planetary exploration missions. He has an S.B. in Aeronautics and Astronautics from MIT, an M.S. in Aerospace Engineering from George Washington University, and a Ph.D. in Aerospace Engineering from Virginia Tech.

Robert D. Braun is the David and Andrew Lewis Associate Professor of Space Technology in the Guggenheim School of Aerospace Engineering at the Georgia Institute of Technology. As Director of Georgia Tech's Space Systems Design Laboratory, he leads a research program focused on the design of advanced flight systems and technologies for planetary exploration. He is responsible for undergraduate and graduate level instruction in the areas of space systems design, astrodynamics, and planetary entry. Prior to coming to Georgia Tech, he served on the technical staff of the NASA Langley Research Center for sixteen years, where he contributed to the design, development, test, and operation of several robotic space flight systems. He has worked extensively in the areas of entry system design, planetary atmospheric flight, and mission architecture development. Dr. Braun is an AIAA Fellow and the principal author or co-author of over 100 technical publications in the fields of planetary exploration, atmospheric entry, multidisciplinary design optimization, and systems engineering. He has a B.S. in Aerospace Engineering from Penn State University, a M.S. in Astronautics from George Washington University, and a Ph.D. in Aeronautics and Astronautics from Stanford University.